

www.acsnano.org

Orientation of Individual Anisotropic Nanocrystals Identified by Polarization Fingerprint

Severin Lorenz, Jan Bieniek, Christian S. Erickson, Daniel R. Gamelin, Rachel Fainblat, and Gerd Bacher*



Cite This: ACS Nano 2021, 15, 13579-13590



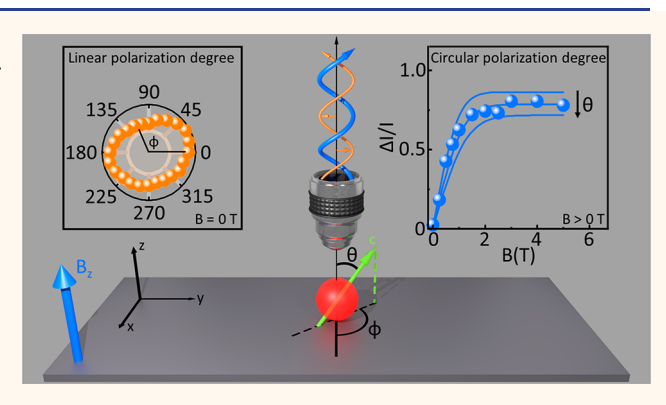
ACCESS

Metrics & More

Article Recommendations

s Supporting Information

ABSTRACT: The polarization of photoluminescence emitted from anisotropic nanocrystals directly reflects the symmetry of the eigenstates involved in the recombination process and can thus be considered as a characteristic feature of a nanocrystal. We performed polarization resolved magneto-photoluminescence spectroscopy on single colloidal $\rm Mn^{2+}:CdSe/CdS$ coreshell quantum dots of wurtzite crystal symmetry. At zero magnetic field, a distinct linear polarization pattern is observed, while applying a magnetic field enforces circularly polarized emission with a characteristic saturation value below 100%. These polarization features are shown to act as a specific fingerprint of each individual nanocrystal. A model considering the orientation of the crystal \vec{c} axis with respect to the optical axis



and the magnetic field and taking into account the impact of magnetic doping is introduced and quantitatively explains our findings. We demonstrate that a careful analysis of the polarization state of single nanocrystal emission using the full set of Stokes parameters allows for identification of the complete three-dimensional orientation of the crystal anisotropy axis of an individual nanoobject in lab coordinates.

KEYWORDS: single nanocrystal spectroscopy, polarization, Stokes polarimetry, nanocrystal orientation, Mn^{2+} :CdSe/CdS, excitonic magnetic polaron, magnetization fluctuation

The information carried by the polarization state of light is harnessed in a wide variety of applications, ranging from emerging modern technologies such as quantum information technology¹⁻⁶ or spintronics⁷⁻⁹ to material characterization of organic^{10,11} or inorganic matter.¹² A particularly intriguing aspect is its use in optical spectroscopy on nanoscale materials, such as two-dimensional transitionmetal dichalcogenides, 13-15 one-dimensional (1D) nanowires¹⁶ and zero-dimensional quantum dots (QDs),¹⁷⁻¹⁹ because the polarization encodes the fingerprint of the electronic eigenstate symmetry.²⁰ A prominent example is the emergence of linearly polarized photoluminescence (PL), for example, induced by a break of rotational symmetry in colloidal QDs (cQDs), 21 by strong shape anisotropies in quantum rods,²² or by the crystal structure in lead halide perovskites.^{23,24} Circularly polarized PL, on the other hand, is widely used to access the magnetic-field-dependent state splitting in undoped ^{23,25-32} as well as in doped QDs. ³³⁻⁴² This state splitting is evidenced by a spectral shift of the right circularly polarized (σ^+) and the left circularly polarized (σ^-)

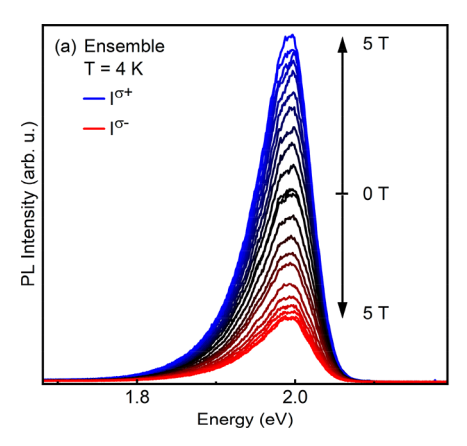
PL and causes an increase of the degree of circular polarization with magnetic field because of the resulting state occupation. Thus, circularly polarized PL is considered as a particularly effective tool for probing magnetic-field-dependent changes of the eigenstate symmetry.⁴³

In undoped cQDs, however, large magnetic fields are typically necessary to reach polarization saturation even at low temperatures because of the small g-factors. Magnetically doped cQDs like Mn²⁺:CdSe cQDs, in contrast, exhibit huge effective g-factors ^{44–46} due to the sp-d exchange interactions between the delocalized charge carriers of the host material (s-type electrons and p-type holes) and the localized magnetic

Received: May 26, 2021 Accepted: July 27, 2021 Published: August 2, 2021







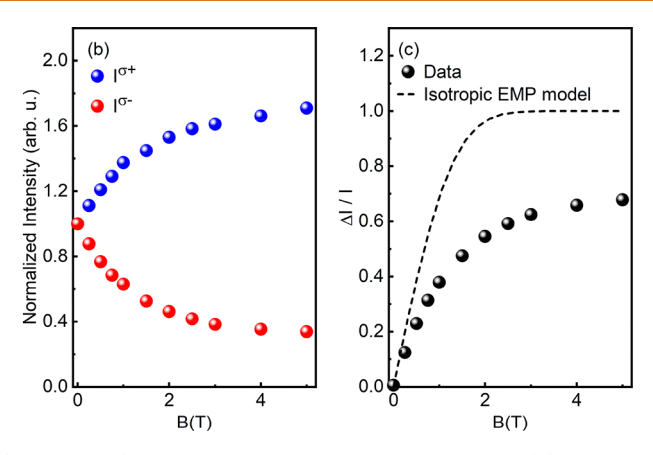


Figure 1. (a) Magneto-PL spectra of σ^+ (black to blue) and σ^- (black to red) polarized ensemble PL, collected at 4 K. (b) Integrated intensity of right circularly polarized emission (I^{σ_+} , blue) and left circularly polarized emission (I^{σ_-} , red) normalized to the corresponding value at B=0 T, and (c) $\Delta I/I$ as a function of the applied magnetic field. The dashed line shows the result for a simulation using a model of isotropic EMP formation.³⁵

moments of the dopants' d electrons. These exchange interactions lead to giant magneto-optical responses 44,47 and strong circularly polarized emission even at small magnetic fields, 48 resulting in the observation of giant Zeeman splittings up to room temperature. 45,49,50 In case of a careful adjustment of the bandgap with respect to the internal ${}^{4}\Gamma_{1}$ $-{}^{6}A_{1}$ Mn^{2+} transition,⁵¹ such materials can exhibit the formation of a spontaneous collective magnetization of the dopant magnetic moments in the presence of an electron-hole pair, mediated by the exchange field between the dopant magnetic moments and the host charge carriers. This so-called excitonic magnetic polaron (EMP) formation has been observed in a variety of DMS systems, ranging from quantum wells⁵²⁻⁵⁵ and selfassembled QDs^{56,57} to cQDs.^{35,58-60} While it is commonly agreed that the exchange field is strong enough to drive the Mn²⁺ magnetization close to saturation at cryogenic temperatures, magnetic fluctuations inhibit the saturation of the degree of circular polarization at small magnetic fields. 35,60

Saturation values of the degree of circular polarization of 100% are usually found for epitaxially grown samples exhibiting EMP formation such as quantum wells $^{52-55}$ and self-assembled QDs. 56,57 Surprisingly, for colloidal nanostructures, such as nanoplatelets 36,38,40 and cQDs with wurtzite crystal structure, saturation values below 100% are consistently found. 35,59 Similarly, saturation values of the degree of circular polarization below 100% have been observed in undoped CdSe cQDs 26,61,62 and were attributed to the anisotropy of the cQDs induced by the wurtzite \vec{c} axis. Reports to date are restricted to ensemble investigations on colloidal nanostructures, which lead to an averaging of nanocrystal orientation, thus hiding polarization fingerprints of individual species.

Here we report on polarization resolved magneto-PL spectroscopy of single wurtzite Mn²⁺:CdSe/CdS core—shell cQDs. We find a distinct linear polarization pattern at zero magnetic field typical for each nanocrystal and circularly polarized PL evolving in a magnetic field with a characteristic saturation of the degree of circular polarization below 100%. Model calculations evidence how the orientation of the crystal \vec{c} axis plays a crucial role for the polarization emitted from each single cQD. We demonstrate the need to measure the full set of Stokes parameters for describing the complete polarization state of the single cQD PL and show how these parameters can be used to determine the three-dimensional (3D) orientation of a single nanoobject in the fixed lab reference frame.

RESULTS AND DISCUSSION

Ensemble of cQDs. Mn²⁺:CdSe/CdS cQDs with a dopant concentration of 3% were synthesized by diffusion doping methods detailed previously (see Supporting Information for general sample analysis). 35,45,46,60 Figure 1a depicts the polarization resolved magneto-PL spectra of an ensemble of Mn²⁺:CdSe/CdS cQDs, dropcast onto a silicon substrate, at T = 4 K. These cQDs exhibit strong EMP formation, as discussed in the Supporting Information. Starting from B = 0 T, where the right circularly polarized $(I^{\sigma+})$ and left circularly polarized $(I^{\sigma-})$ PL intensities are identical, $I^{\sigma+}$ (black to blue) continuously increases with B, while $I^{\sigma-}$ (black to red) decreases. However, even at B = 5 T, I^{σ} -does not vanish. Interestingly, we find no energy splitting between the σ^+ and σ^- components of the PL spectra in Figure 1a within the resolution of the experiment. This observation is in pronounced contrast to the oppositely directed energy shift for σ^+ and σ^- polarized PL typically observed in epitaxially grown QDs, which is usually explained by two involved states of opposite spin orientation, leading to two Zeeman split branches. 48,53,63-65

Plotting the integrated intensities normalized to its value at B = 0 T (Figure 1b) reveals a saturation of $I^{\sigma+}$ and $I^{\sigma-}$ at 170% and 30% of their starting values, respectively. Note that the sum of $I^{\sigma+}$ and $I^{\sigma-}$ is constant, hinting toward a magnetic fieldinduced redistribution of populations between two emissive states of different symmetry. From the integrated intensities, we determine the degree of circular polarization, $\Delta I/I = (I^{\sigma +} I^{\sigma-})/(I^{\sigma^+}+I^{\sigma-})$, plotted in Figure 1c. For small magnetic field strengths (B < 1 T), $\Delta I/I(B)$ increases steeply, followed by a saturation behavior at about 70% for high magnetic fields. In literature, saturation values of 100% have been reported in DMSs with EMP formation such as quantum wells⁵²-55 or selfassembled QDs^{56,57} and even in epitaxially grown DMS QDs in the absence of EMP formation. 48 On the other hand, finite saturation values between 50% and 80% have been published for colloidal DMS nanoplatelets^{36,38,40} as well as for wurtzite cQDs with EMP formation.^{35,59} One similarity between all these systems is the presence of an axis of anisotropy, which is either introduced by the growth mechanism or by the crystal structure. A major difference, however, is the orientation of this axis of anisotropy: It is predefined by the growth mechanism in epitaxial quantum wells and self-assembled QDs but randomly

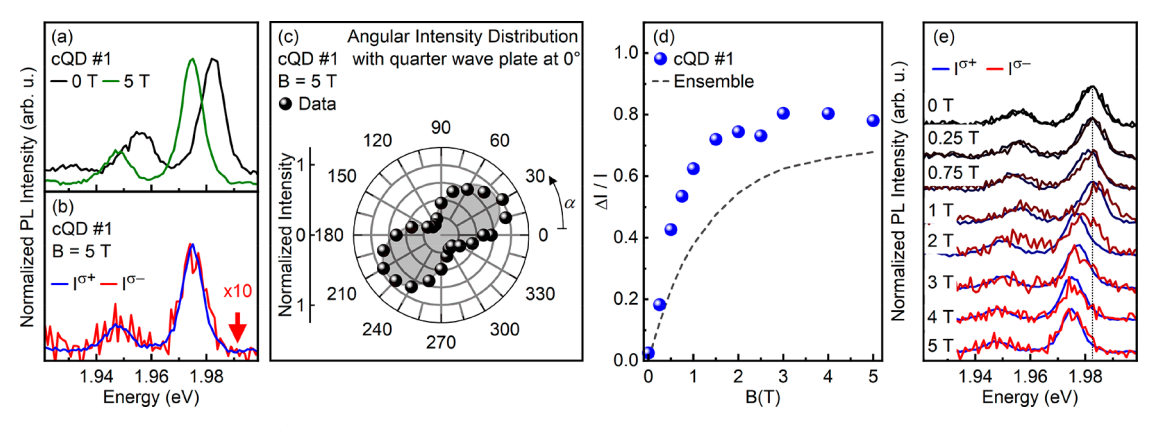


Figure 2. PL of a single cQD at 4 K. (a) Normalized PL spectra (without polarization resolution) in the presence and absence of a magnetic field of 5 T. (b) Normalized PL spectra for σ^+ and σ^- polarization at 5 T. (c) Integrated PL intensity $I(\alpha)$ of cQD #1 using a quarter wave plate with its fast axis horizontal to the table (defined as angle $\alpha=0^\circ$) and a rotatable linear polarizer with transmission axis at an angle α . Each radial tick equals an intensity step of 0.25. The shaded area serves as a guide to the eye. (d) $\Delta I/I(B)$ for cQD #1 (symbols) compared to the ensemble data (dashed line). (e) Normalized magnetic-field-dependent spectra of σ^+ -polarized (black to blue) and σ^- -polarized (black to red) PL of cQD #1. Spectra have been stacked along the y axis for clarity.

oriented in ensembles of cQDs and colloidal nanoplatelets. Thus far, for colloidal DMS nanocrystals, no conclusive explanation has been given for the saturation of $\Delta I/I < 100\%$. However, it has been hypothesized 35,59 that anisotropy effects, which are averaged due to the random orientation of the crystal \vec{c} , may play a role in determining $\Delta I/I$, similar to the case of undoped cQDs. 26,61,62

Single cQDs. Acknowledging that the individual anisotropy axes, caused, for example, by crystal and/or shape anisotropy, are oriented arbitrarily in an ensemble of cQDs, we conducted confocal polarization-resolved micro-PL spectroscopy on selected single Mn²⁺:CdSe/CdS core-shell cQDs at 4 K. Figure 2a plots the PL of a single cQD (cQD #1) in absence and presence of a magnetic field of 5 T. The spectra exhibit a dominant feature at 1.982 eV and a weaker one, shifted by 26 meV to lower energies. These features are unambiguously assigned to the zero phonon line (ZPL) and its first phonon replica due to the simultaneous emission of a photon and a longitudinal optical phonon (1-LO).66,67 The broad full width at half maximum (fwhm) of about 8.5 meV is caused by magnetic fluctuations and has been discussed elsewhere. 60 The energetic position of the ZPL at 5 T shows a clear red shift of 7 meV with respect to its position at 0 T. Surprisingly, and in accordance with our observations in the ensemble PL, we find no spectral shift between the σ^+ and σ^- polarized PL components at 5 T (see Figure 2b), although the ratio $I^{\sigma+}/I^{\sigma+}$ $I^{\sigma-} \sim 10$, that is, the PL emission at 5 T is strongly circularly

To verify the strong circular polarization, a combination of a quarter wave plate with its fast axis oriented horizontally relative to the table (defined as $\alpha=0^{\circ}$) and a rotatable analyzing linear polarizer was used. Figure 2c plots the corresponding normalized angular dependence $I(\alpha)$ of the integrated spectral intensity, where α is the angle of the analyzer transmission axis with respect to the table plane. In this configuration, the quarter wave plate converts σ^{+} (σ^{-}) polarized light into linearly polarized light, detected at an angle of +45° (315°, i.e., -45°). After passing the quarter wave plate, $I(\alpha)$ exhibits the dumbbell-shaped profile expected for dominantly linearly polarized light. This demonstrates the strong circularly polarized character of the PL before passing the quarter wave plate. Identifying $I^{\sigma^{+}} = I(45^{\circ})$ and $I^{\sigma^{-}} = I(45^{\circ})$

 $I(135^\circ)$, we find a value for the circular polarization degree of $\Delta I/I = 78\%$ at 5 T. Figure 2d compares $\Delta I/I(B)$ for cQD #1 and the ensemble. $\Delta I/I(B)$ rises much steeper for cQD #1 than for the ensemble and saturates at higher values. This result suggests that the slope and the saturation value are individual signatures of a cQD and its particular orientation on the substrate.

We emphasize that the lack of an energetic splitting between the σ^+ and σ^- polarized components of the PL at B=0 T (see Figure 2b) is quite surprising. In fact, in self-assembled single DMS QDs both with and without EMP formation, energetic splittings between the σ^+ and σ^- ZPL have been observed. In the absence of EMP formation, the large energy splitting of 20 meV/T has been attributed to the giant Zeeman splitting induced by the magnetic field due to strong sp-d exchange interactions between the dopant d electrons and the host charge carriers.⁴⁸ In the case of EMP formation, the smaller energy splitting of 3 meV/T has been attributed to EMPs, formed either parallel or antiparallel to the magnetic field direction. 39,65 A similar energy splitting between $I^{\sigma+}$ and $I^{\sigma-}$ is observed below 2 T, and even a slight blueshift of $I^{\sigma-}$ with B is obtained (see Figure 2e), suggesting that in this regime the PL stems from the two EMP states as discussed above. For higher magnetic fields, the red shift observed for both, $I^{\sigma+}$ and $I^{\sigma-}$ with respect to B = 0 T is similar, although the intensity is quite different (see Figure 2b). We therefore hypothesize that at high magnetic fields, σ^+ as well as σ^- components of the PL are actually emitted from one and the same EMP state (see Supporting Information for a detailed discussion). This is quite surprising as a magnetic field of 5 T is expected to lead to a complete depopulation of the upper Zeeman branch and the PL should be fully circular polarized.

To explain the unsual polarization properties of the PL in Mn²⁺-doped single nanocrystals, it is therefore necessary to consider the state occupation due to the Zeeman splitting of the contributing states, the magnetic doping, and the crystal anisotropy. It is instructive to start by subsequently describing the magnetic-field-dependent state occupation for undoped cQDs, the impact of magnetic doping and magnetic fluctuations, and the consequence of EMP formation on the polarization state of the emission in wurtzite cQDs.

Degree of Polarization for Undoped CdSe cQDs. For undoped CdSe cQDs, the relevant optically active excitonic states for the PL emission are the ones dominated by their heavy hole (HH) $|\pm 3/2\rangle$ and electron $|\mp 1/2\rangle$ states. Here, the excitonic states are split in a magnetic field by the intrinsic Zeeman splitting $\Delta E_{Z,int}$, which is on the order of 0.1 meV/ T.61 As the magnetic field increases, the energy splitting between the two spin split branches with opposite symmetry increases, leading to a change in state occupation. In case the spin flip rate between these states exceeds the recombination rate significantly, the relative contributions of these states to the PL signal can be deduced assuming thermal equilibrium at the moment of exciton recombination, described by a Boltzmann distribution with $\Delta E_{Z,int}$ as the energetic separation of the states. For undoped cQDs with wurtzite symmetry, the total angular momentum of the HH state is constrained parallel to the crystal \vec{c} axis with opposite projections corresponding to the $|\pm 3/2\rangle$ states. As a consequence, the emitted light from excitons including these states has opposite helicity, depending on the angle θ between the crystal \vec{c} axis and the direction of observation \vec{k} . The relative intensities of σ^+ and σ^- emitted light are then given by 26,61,62

$$I_{|+3/2,-1/2\rangle}^{\sigma^{\pm}} \propto (1 \pm \cos(\theta))^2$$
 (1a)

$$I_{-3/2,+1/2}^{\sigma^{\pm}} \propto (1 \mp \cos(\theta))^2$$
 (1b)

where we imply recombination of holes in the $|\pm 3/2\rangle$ states with electrons in the $|\mp 1/2\rangle$ states. Combined with the occupation of the Zeeman split states due to the Boltzmann distribution, the ensemble average over all possible angles of crystal orientation with respect to the observation axis theoretically yields a saturation value of $\Delta I/I \sim 75\%$, which, depending on the cQD size and material, can only be reached at extremely high magnetic fields on the order of 50 T or higher. It should be noted that here, the direction of the charge carrier's angular momentum at the moment of radiative recombination is of fundamental importance for the PL polarization.

The Case of Magnetically Doped cQDs. In magnetically doped cQDs exhibiting sp-d exchange, an analogous approach can be used by replacing the intrinsic Zeeman splitting with the giant Zeeman splitting, which can be written as $\Delta E_{\rm sp-d} = g_{\rm eff}\mu_{\rm B}B_{\rm s}^{44-46}$ with $\mu_{\rm B}$ representing the Bohr magneton. Here, all exchange effects are included in the effective gyromagnetic ratio g_{eff} which can reach values up to 1180 at low temperatures and small magnetic fields. 45,46 Such large exchange interactions yield Zeeman splittings up to several tens of meV/T. Due to the very effective ordering of the Mn²⁺ spins in a magnetic field at low temperatures, the giant Zeeman splitting increases rapidly with B (paramagnetic behavior), leading to a much more sensitive change in state occupation with B and therefore to a steeper increase of $\Delta I/I(B)$ compared to the undoped (diamagnetic) case. 48 Note that the state occupation, and thus the degree of circular polarization, in undoped and doped cQDs is determined by the Zeeman splitting at the moment of radiative recombination, which is usually described by a thermal equilibrium Boltzmann distribution in cases where the spin relaxation rate exceeds the recombination rate.

Magnetically Doped cQDs with EMP Formation: Isotropic Case. To derive the polarization degree of cQDs with EMP formation, one has to consider the complete

formation process, including the EMP direction. In case of EMP formation, the collective alignment of the Mn²⁺ magnetic moments inside the effective exciton volume $V_{\rm eff}$ is driven by the internal exchange field $\vec{B}_{\rm exc} = \vec{B}_{\rm exc}^{\rm el} + \vec{B}_{\rm exc}^{\rm h}$ with orientations given by the direction of the charge carriers' total angular momentum (see Supporting Information). In Mn²⁺-doped II-VI QDs, it is commonly assumed that the instantaneous direction of the Mn²⁺ magnetization $M_f = M_{Mn}(t=0)$ at the moment of exciton creation determines the direction of EMP formation, leading to an isotropic model of EMP formation. Due to the quantum mechanical nature, the Mn²⁺ magnetization is subject to fluctuations in magnitude and direction, and has to be described by the joint probability distribution function $\Phi(M_{Mn})$ (see Supporting Information for details), describing the chance to find a certain value for M_{Mn} . Using this framework, the PL polarization can be calculated using eqs 1a and 1b, where the angle θ is now given by the angle between the EMP direction and the magnetic field direction. In Faraday geometry, that is, direction of light propagation k and magnetic field B are parallel, $\Delta I/I$ can then be calculated by ³⁵

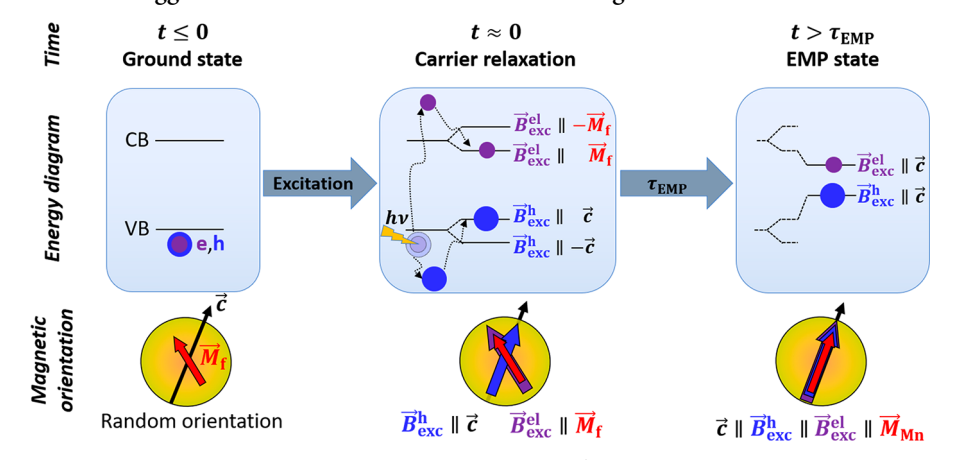
$$\Delta I/I = \frac{\int dM_{x} dM_{y} dM_{z} (I^{\sigma +} - I^{\sigma -}) \Phi(M_{x}, M_{y}, M_{z})}{\int dM_{x} dM_{y} dM_{z} (I^{\sigma +} + I^{\sigma -}) \Phi(M_{x}, M_{y}, M_{z})}$$
(2)

The dashed line in Figure 1c shows the result for a simulation using literature parameters for similar cQDs (see Supporting Information). Apparently, this model of isotropic EMP formation consequently overestimates the increase of $\Delta I/I$ for small magnetic fields and cannot explain the saturation $\Delta I/I < 100\%$ at high magnetic fields in cQDs. Therefore, a model explicitly incorporating anisotropy effects needs to be developed.

Magnetically Doped cQDs with Anisotropic EMP Formation: Case of Zero Magnetic Field. We therefore establish a model for describing the PL polarization considering anisotropy effects. Note that the direction of any axis of anisotropy is by default specific to each single cQD in lab coordinates. It is therefore necessary to start the description at a single particle level and move toward an ensemble by averaging afterward. $\vec{B}_{\rm exc}^{\rm el}$ is commonly assumed to be directed by $M_{\rm Mn}$ due to the isotropic orbital s character of the electron wave function. ⁶⁸ However, even in the fully formed EMP state, $\vec{B}_{\rm exc}^{\rm h}$ can be constrained by an axis of anisotropy in wurtzite cQDs.⁶⁰ This constraint is thought to be caused by the strong anisotropic orbital p character of the hole wave function. The consequences of this strong anisotropic behavior of the hole exchange field for the initial mechanism of EMP formation, and ultimately the PL polarization degree, are therefore discussed in the following.

As $\vec{B}_{\rm exc}^{\rm h}$ is constrained by the cQD anisotropy axis, it is reasonable to assume that this constraint is already established at the moment of exciton generation, that is, at $t \approx 0$. A plausible source of the dominant anisotropy axis in wurtzite cQDs is the crystal \vec{c} axis (see Supporting Information for a discussion of relevant energy scales). Then, the direction of the hole exchange field is respectively given by $\vec{B}_{\rm exc}^{\rm h} \parallel \vec{c}$ and $\vec{B}_{\rm exc}^{\rm h} \parallel -\vec{c}$. This first-order criterion is then superimposed with the second order influence of minimizing the p-d exchange energy for the hole $E_{\rm p-d}(t\approx 0) = -V_{\rm eff}\vec{M}_{\rm f} \cdot \vec{B}_{\rm exc}^{\rm h}$. It is therefore energetically favorable for the hole to align its exchange field in the direction that yields an energy gain $\Delta E_{\rm p-d} < 0$, that is, the direction with positive projection $(\vec{M}_{\rm f} \cdot \vec{B}_{\rm exc}^{\rm h}) > 0$. In other words, while the crystal \vec{c} axis predefines two possible

Scheme 1. Illustration of the Suggested EMP Formation Process for a Single Excitation Event at B = 0 T^a



"This schematic depicts the EMP formation for a randomly chosen case of $M_c = \vec{M}_f \cdot \vec{c} > 0$ at the moment of photoexcitation (t = 0).

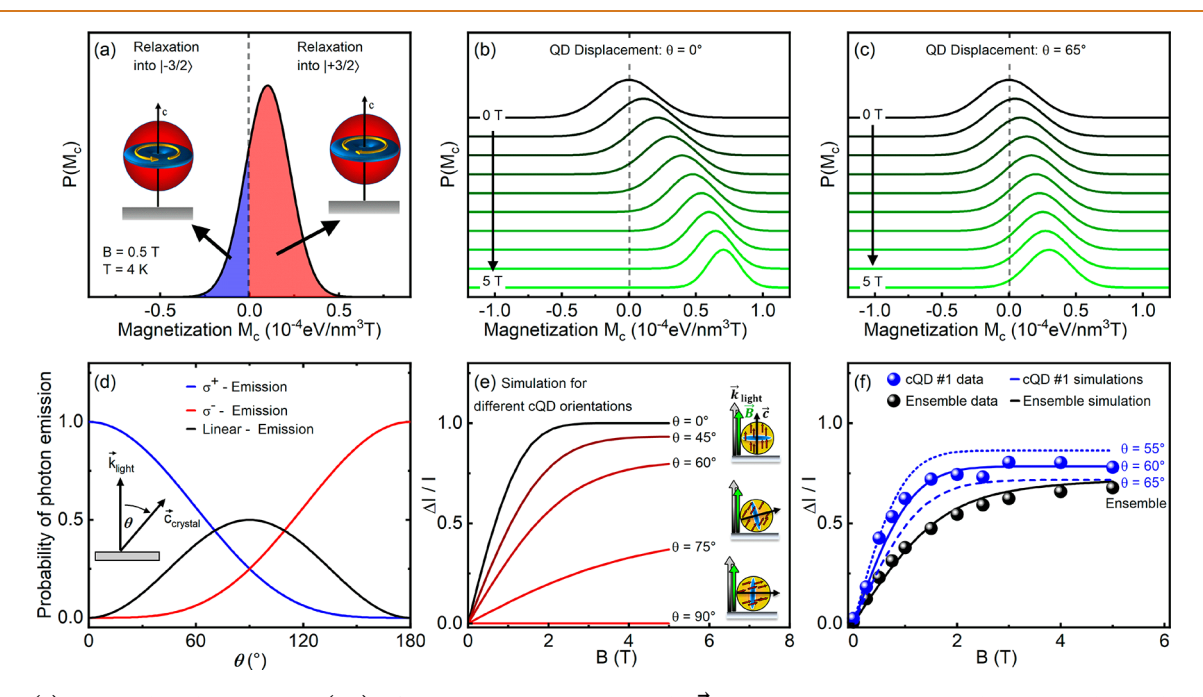


Figure 3. (a) Probability distribution $P(M_c)$ of the magnetization along the \vec{c} direction at B=0.5 T. The blue and red shaded areas correspond the probabilities of HH relaxation into the $|-3/2\rangle$ and $|+3/2\rangle$ states, respectively. (b) Calculated change of the probability distribution $P(M_c)$ in a magnetic field applied along \vec{z} for $\theta=0^\circ$ and (c) $\theta=65^\circ$ at different magnetic field strengths. (d) Probability of detecting different PL polarization from recombination of a $|+3/2\rangle$ hole and a $|-1/2\rangle$ electron for a cQD with its \vec{c} axis displaced by an angle θ from the direction of light propagation \vec{k} ($\vec{k}||\vec{z}$). (e) Simulated $\Delta I/I(B)$ for five differently oriented cQDs. (f) Comparison of $\Delta I/I$ vs B for cQD #1 (blue symbols) with three different simulations for a single cQD using $\theta=55^\circ$ (blue dotted line), 60° (blue solid line), and 65° (blue dashed line) as well as ensemble data shown in Figure 1 (black symbols) in comparison with a simulation for the whole ensemble of cQDs (black line). For parameters used in the simulations, see Supporting Information.

directions of $\vec{B}_{\underline{exc}}^{h}$ the initial direction of the fluctuating magnetization \vec{M}_{f} at the moment of exciton generation determines the preferred case out of those two.

Scheme 1 illustrates the suggested EMP formation process for one photoexcitation event. In the case depicted here, the instantaneous magnetization $\vec{M}_{\rm f}$ is oriented toward the top-left at the moment of photoexcitation and \vec{c} is oriented to the top right. Then the magnetization component in the direction of \vec{c} , $M_{\rm c} = \vec{M}_{\rm f} \cdot \vec{c}$, is positive. Therefore, the state with $\vec{B}_{\rm exc}^{\rm h}$ parallel to \vec{c} is energetically favored, and the subsequent HH relaxation leads to $\vec{B}_{\rm exc}^{\rm h}$ parallel to \vec{c} under the assumption that the HH spin relaxation is fast compared to EMP formation. Note that for another excitation event, where $M_{\rm c}$ is negative, the

relaxation would occur into the state with $\vec{B}_{\rm exc}^{\rm h}$ antiparallel to \vec{c} . The electron, on the other hand, has an isotropic character and can either relax into the direction of $\vec{M}_{\rm f}$ to maximize the energy gain by magnetic s-d exchange interaction or (if $|\vec{M}_{\rm f}|$ is small) relax into the direction of $\vec{B}_{\rm exc}^{\rm h}$ to maximize the energy gain due to the electron—hole s-p exchange interaction. After the hole is relaxed with $\vec{B}_{\rm exc}^{\rm h} ||\vec{c}$ or $\vec{B}_{\rm exc}^{\rm h}||-\vec{c}$, the Mn²⁺ spins align into the direction of $\vec{B}_{\rm exc}^{\rm h}$ and the EMP is formed. During the EMP formation, the magnetization reaches saturation, and the energy of the electron—hole pair is lowered by the EMP binding energy, splitting the $|\pm 3/2\rangle$ states substantially in energy and preventing thermal occupation of the upper state. Therefore, the problem of predicting EMPs formed with either

the $|+3/2\rangle$ or $|-3/2\rangle$ HH state, from which finally the PL polarization can be derived, is reduced to determining the probability for $M_c > 0$ based on the statistics given above.

Magnetically Doped cQDs with Anisotropic EMP Formation: Case of Finite Magnetic Field. With $\vec{B} \parallel \vec{z}$, the orientation of a single cQD with crystal axis \vec{c} with respect to \vec{z} is characterized by its polar angle θ between \vec{c} and \vec{z} . The above framework can then be used to determine the number of EMPs formed in either the \vec{c} or $-\vec{c}$ direction by determining the probability of $M_c > 0$ and the probability of $M_c < 0$. It is instructive to first consider the special case of $\vec{c} \parallel \vec{z}$, that is, $\theta = 0^\circ$. Then, M_c is given by M_z , and the task is simply to determine the probability of finding \vec{M}_f with positive component M_z along \vec{z} , using the probability distribution $P(M_z)$, which describes only the z component of \vec{M}_f instead of the full joint probability distribution $\Phi(M_x M_{yz} M_z)$:

$$P(M_z) = \frac{1}{\sqrt{2\pi\langle\delta M_z^2\rangle}} \exp\left(-\frac{(M_z - \langle M_z \rangle)^2}{2\langle\delta M_z^2\rangle}\right)$$
(3)

Then, the portion of HH relaxation with $\vec{B}_{\rm exc}^{\rm h}$ pointing to the positive \vec{z} direction, and hence subsequent EMP formation in this direction, is obtained by summing the probability K for M_z > 0, that is:

$$K = \int_0^\infty P(M_z) dM_z = \frac{1}{2} \left[1 - \text{erf} \left(-\frac{\langle M_z \rangle}{\sqrt{2 \langle \delta M_z^2 \rangle}} \right) \right]$$
(4)

The corresponding portion of HH relaxation with $\vec{B}_{\rm exc}^{\rm h}$ pointing in the negative z direction and subsequent EMP formation in this direction is given by the integral with limits $(-\infty,0)$, or, since $P(M_z)$ is normalized, simply by (1-K). Figure 3a plots $P(M_c) = P(M_z)$ for $\theta = 0^\circ$ at B = 0.5 T and T = 4 K. The red and blue shaded areas nicely visualize $P(M_c > 0)$ and $P(M_c < 0)$ and thus the relaxation probability for the HH with $\vec{B}_{\rm exc}^{\rm h} ||\vec{c}|$ and $\vec{B}_{\rm exc}^{\rm h} ||\vec{c}|$ and $\vec{B}_{\rm exc}^{\rm h} ||\vec{c}|$ are spectively. The inset schematically shows the donut-like shape of the heavy hole wave function with total orbital momentum projections $J_z = \pm 3\hbar/2$.

To visualize the influence of the magnetic field, Figure 3b depicts $P(M_c)$ for different magnetic fields applied in \vec{z} -direction. With increasing magnetic field, the distribution is shifted toward positive values of M_z and narrowed. The shift indicates an increase in the time averaged expectation value of the magnetization $\langle M_c \rangle = \langle M_z \rangle$, and the decrease of the fwhm corresponds to a suppression of fluctuations $\langle \delta M_c^2 \rangle = \langle \delta M_z^2 \rangle$. From Figure 3b, it becomes obvious that the probability that $M_c > 0$ grows with applied magnetic field, making relaxation into the HH state $|+3/2\rangle$ with $\vec{B}_{\rm exc}^{\rm h}||\vec{c}|$ increasingly likely. For magnetic fields larger than 2 T, practically all EMPs are formed along the positive \vec{z} direction, which, as we will discuss below, corresponds to a saturation of the PL polarization.

Before the consequences for the PL polarization are considered, the general case of a cQD with crystal orientation $\vec{c} \nmid \vec{z}$, that is, $\theta \neq 0^\circ$ needs to be discussed. In this case, $M_c = \cos(\theta) M_z$ and the probability to find \vec{M}_f with positive component along \vec{c} can be found in a similar way as before, but with a modified version of eqs 3 and 4. Without an electron—hole pair present, the axial anisotropy splitting for the Mn²⁺ spins in wurtzite CdSe cQDs has previously been determined by means of electron paramagnetic resonance spectroscopy. The axial zero-field splitting parameter D was found to be smaller than 0.01 cm⁻¹. Therefore, the total the

Mn²⁺ ground-state zero-field splitting of 6D is in the order of only a few percent of the thermal energy $k_{\rm B}T$ at 4 K, and thus the Mn²⁺ spin orientation at 4 K is not influenced by the crystal anisotropy. Hence, the joint probability distribution $\Phi(M_{\rm x}M_{\rm y}M_{\rm z})$ is independent of θ and describes a 3D Gaussian distribution, which, in the presence of a magnetic field in \vec{z} direction, is displaced along \vec{z} and narrowed. In analogy to the approach above, the probability of finding $M_{\rm c} > 0$ for $\vec{c} || \vec{z} ||$ is described by a 1D probability distribution $P(M_{\rm c})$, reflecting the probability of magnetization along \vec{c} . The modified version of eq 4 describing the probability of EMP formation in the direction of \vec{c} is then given by (see Supporting Information for details):

$$K = \frac{1}{2} \left[1 - \operatorname{erf} \left(-\frac{\langle M_{z} \rangle \cos(\theta)}{\sqrt{2} \cos(\theta) \sqrt{\langle \delta M_{\parallel}^{2} \rangle} + \sqrt{2} \sin(\theta) \sqrt{\langle \delta M_{\perp}^{2} \rangle}} \right) \right]$$
(5)

where $\langle \delta M_\parallel^2 \rangle$ and $\langle \delta M_\parallel^2 \rangle$ are the magnetic fluctuations parallel and perpendicular to the magnetic field. To demonstrate the consequences of a finite angle $\theta \neq 0^\circ$, Figure 3c plots $P(M_c)$ for an angle of $\theta = 65^\circ$ with the same parameters as used for the case of $\theta = 0^\circ$ in Figure 3b. The reduced shift of $P(M_c)$ as well as the reduced narrowing with magnetic field are clearly visible, leading to a significant change in the probabilities of HH relaxation with $\vec{B}_{\rm exc}^{\rm h}$ directed along \vec{c} and thus a reduced probability of EMP formation in this direction. This results in a finite probability of EMP formation along $-\vec{c}$ even at 5 T. Thus, increasing the angle θ mitigates the influence of the external magnetic field, leading to a weaker dependence of the probability of EMPs formed along \vec{c} , and thus to a more gradual increase of $\Delta I/I(B)$.

We note the similarity between this model of constrained EMP orientation to the case of undoped cQDs, where the direction of the total angular momentum during HH relaxation is also determined by the crystal \vec{c} axis. In this latter case, the probability of excitons with total angular momentum along \vec{c} or $-\vec{c}$ is given by the thermal occupation of the Zeeman split electronic states and described by the equilibrium Boltzmann distribution. Such a thermal occupation cannot be used for the fully formed EMP state because of the very large energies involved. Instead, eq 5 has to be used to give the magnetic field dependent relative intensities of PL emitted from EMPs oriented along \vec{c} or $-\vec{c}$ for any given cQD orientation, characterized by its polar angle θ .

It is commonly recognized that the helicity of emitted photons during the recombination process is a direct result of the preservation of angular momentum. For example, recombination of a hole in the $|+3/2\rangle$ state with total angular momentum projection $I_z = +3\hbar/2$ and an electron in the |-1/2|2) state with total angular momentum projection $-\hbar/2$ yields a photon with angular momentum + \hbar , that is, a σ^+ polarized photon. Due to the conservation of angular momentum, the reference axis of this photon, however, is given by the reference axis of the recombining electron-hole pair, in our case the crystal \vec{c} axis of the cQDs. As a consequence, the observation of the photon yields an elliptical polarization that depends on the angle between \vec{c} and the observation direction \vec{k} . Since all experiments are conducted in Faraday geometry, that is, $k||\vec{B}||\vec{z}$, this angle is given by the polar angle of the crystal \vec{c} axis, θ . Figure 3d plots the angle dependence of the PL polarization for the recombination of a $|+3/2\rangle$ HH with a $|-1/2\rangle$ 2) electron. While for $\theta = 0^{\circ}$ the emission is purely σ^{+}

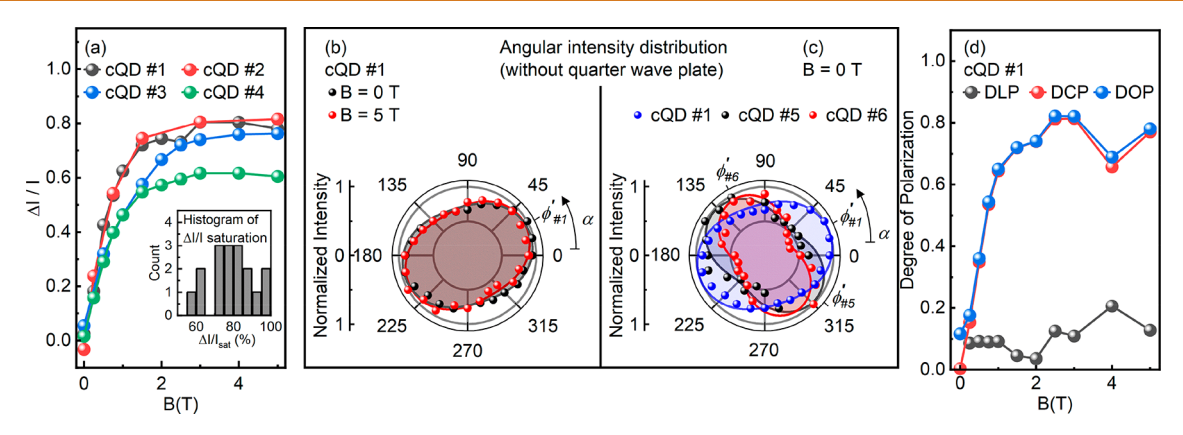


Figure 4. (a) $\Delta I/I(B)$ of four different single cQDs at 4 K. The inset shows a histogram of $\Delta I/I$ saturation values for several single cQDs. (b) Integrated intensity $I(\alpha)$ for cQD #1 at B=0 T (black) and B=5 T (red). (c) Comparison of $I(\alpha)$ for three single cQDs at B=0 T. ϕ' marks the linear polarization orientation angle for the corresponding single cQD. Shaded areas in (b) and (c) serve as guides to the eye. (d) Degree of linear polarization (black), degree of circular polarization (red), and total degree of polarization (blue) for single cQD #1 obtained from measurements of the full Stokes parameters at each magnetic field strength.

polarized, it becomes completely σ^- polarized for $\theta = 180^\circ$. For intermediate angles, the polarization becomes elliptical and even dominantly linear for $\theta = 90^\circ$.

We therefore expect the PL polarization degree after EMP formation along the $+\vec{c}$ axis, that is, after relaxation of the HH into the $|+3/2\rangle$ state, to exhibit the same angle dependence as given by eqs 1a and 1b. Then, the total intensities for σ^+ and σ^- polarized light have contributions from EMPs formed along \vec{c} (called $I_{\uparrow\uparrow}^{c\pm}$) as well as from EMPs formed along $-\vec{c}$ (called $I_{\uparrow\uparrow}^{o\pm}$), that is, $I^{o+} = I_{\uparrow\uparrow}^{o+} + I_{\uparrow\downarrow}^{o+}$ and $I^{o-} = I_{\uparrow\uparrow}^{o-} + I_{\uparrow\downarrow}^{o-}$. The PL intensity $I_{\uparrow\uparrow}$ emitted from EMPs is proportional to the probability of EMP formation parallel to \vec{c} and therefore given by K, and it has contributions from both helicities $I_{\uparrow\uparrow}^{o+}$ and $I_{\uparrow\uparrow}^{o-}$, while the intensity $I_{\uparrow\downarrow}$ is proportional to (1-K) with contributions from $I_{\uparrow\downarrow}^{o+}$ and $I_{\uparrow\downarrow}^{o-}$. Collecting all contributions and weighting them with the probability of EMP formation in the corresponding direction gives the intensities $I^{o+}(\theta)$ and $I^{o-}(\theta)$ emitted from a single cQD:

$$I^{\sigma+}(\theta) = I_{\uparrow\uparrow}^{\sigma+} + I_{\uparrow\downarrow}^{\sigma+}$$

$$= A[K(B, \theta)(1 + \cos(\theta))^{2} + (1 - K(B, \theta))(1 - \cos(\theta))^{2}]$$
(6a)

$$I^{\sigma^{-}}(\theta) = I_{\uparrow\uparrow}^{\sigma^{-}} + I_{\uparrow\downarrow}^{\sigma^{-}}$$

$$= A[K(B, \theta)(1 - \cos(\theta))^{2} + (1 - K(B, \theta))(1 + \cos(\theta))^{2}]$$
(6b)

where A is a constant. Using eqs 6a and 6b, the magnetic field dependence of $\Delta I/I$ can be calculated for a single cQD with orientation θ of the \vec{c} -axis with respect to the laboratory \vec{z} -axis. Figure 3e plots simulated $\Delta I/I(B)$ curves for five differently oriented single cQDs, as illustrated by the inset scheme. Comparison of the five curves yields two major features: First, only cQDs with $\theta = 0^{\circ}$ yield a saturation value of $\Delta I/I = 100\%$, while for those with θ between 0° and 90° , a saturation value between 100% and 0% can be achieved. This result is a direct consequence of the mixed σ^+ and σ^- emission from each state. In the limit of high magnetic fields and for $0^{\circ} < \theta < 90^{\circ}$, where only EMPs with $\vec{B}_{\text{exc}}^{\text{h}} || \vec{c}|$ are formed, the PL intensity is given by $I_{\uparrow\uparrow}$ with right and left circularly polarized contributions $I_{\uparrow\uparrow}^{\sigma+}$ and $I_{\uparrow\uparrow}^{\sigma-}$ depending on the polar angle θ . This situation leads to saturation values of $\Delta I/I$ < 100%. Therefore, the saturation value of $\Delta I/I(B)$ purely depends on the polar angle θ , that is, the orientation of the \vec{c} axis of the cQD with respect to the \vec{z}

direction but not on any other specifics of the material system such as cQD size, dopant concentration, shape anisotropy, etc. The second important observation relates to the changing slope $\Delta I/I(B)$ with θ . This flattening is a direct consequence of the mitigated influence of the magnetic field onto the magnetization components along \vec{c} , leading to a slow increase of $\langle M_c \rangle = \cos(\theta) \langle M_z \rangle$ and a reduced suppression of fluctuations $\langle \delta M_c^2 \rangle$, as discussed in the Supporting Information. Therefore, much stronger magnetic fields are needed to reach polarization saturation for large polar angles θ than for small values of θ . Note that the finite saturation value as well as the reduced slope for low magnetic fields differs for each single cQD orientation. Averaging over all possible directions thus enables the simulation of the expected $\Delta I/I(B)$ curve for the ensemble. The black solid line in Figure 3f depicts such a simulation and shows extremely good agreement with the ensemble data (black symbols) presented in Figure 1 (see Supporting Information for details).

As noted above, once polarization saturation is reached by a sufficiently strong magnetic field, the saturation value of $\Delta I/I$ of a cQD only depends on the polar angle θ . Thus, the simulated $\Delta I/I(B)$ traces can be used to determine the polar angle θ of a real cQD with respect to the lab \vec{z} direction on the substrate surface. Figure 3f compares the data of cQD #1 (blue symbols) with three simulated $\Delta I/I(B)$ traces (blue lines) for single cQDs with $\theta = 55^{\circ}$ (dotted), $\theta = 60^{\circ}$ (solid) and $\theta = 65^{\circ}$ (dashed) (see Supporting Information for detailed simulation parameters). We find very good agreement between the experimental data of cQD #1 and the simulation of $\Delta I/I(B)$ for $\theta = 60^{\circ}$. Additionally, the simulated saturation value strongly depends on the polar angle θ . This result demonstrates how the saturation value of $\Delta I/I(B)$ can be used as an elegant and relieable tool to determine the orientation of a single cQD on a substrate with respect to the optical axis. Note that this idea is not limited to the special case of cQDs with EMP formation but rather can be used to determine the orientation of any anisotropic cQD or similar nanostructure with appropriate electronic structure. Magnetically doped cQDs are just a particularly attractive model system because of the comparably small magnetic fields needed to achieve saturation.

Figure 4a shows $\Delta I/I(B)$ of four different single cQDs. First, the curves exhibit different saturation values for high magnetic

fields between 60% and 80%, suggesting different polar angles θ for each of these cQD's crystal orientations, in agreement with the model above. Interestingly, within a data set of 17 single cQDs, no cQDs with a saturation value below 50% were found (see inset in Figure 4a). This result could be a consequence of preferred cQD orientation due to the single cQD sample preparation, where each single cQD is in contact with the substrate surface, in contrast to the ensemble, where nearly all cQDs are surrounded by other cQDs and a matrix of organic ligands. Because the CdS shell is strongly faceted (see TEM images in Figure S1 of the Supporting Information), a true random orientation of the cQD crystal orientation is therefore likely inhibited.

The second important feature of the $\Delta I/I(B)$ traces is the fact that at zero magnetic field nonzero $\Delta I/I$ values varying between +5% and -5% are observed. This deviation from zero is found to be different for each individual cQD, suggesting a hidden influence, which to the best of our knowledge has not been addressed in literature so far. Following the argumentation given above, the observation of a circularly polarized photon with its angular momentum direction tilted by an angle θ from the observation direction can be either detected as being σ^+ , σ^- , or linearly polarized (π) . Our experiments are conducted in Faraday geometry. This suggests that the single cQD emission, in addition to the above-discussed circularly polarized contributions, also comprise a linearly polarized PL component I^{π} . An analogue consideration is known for the emission from the exciton fine structure state $\pm 1^{L}$ in wurtzite cQDs, where a linearly polarized PL component with an angular dependence $I_{\pm 1}^{\pi}(\theta) \propto \sin^2(\theta)$ was found.²⁰

Figure 3d shows the dependence of the π -polarized PL component, which is zero at $\theta = 0^{\circ}$ and 180° and has its maximum value at $\theta = 90^{\circ}$. This behavior can be understood by recognizing that the electric field of circularly polarized PL emitted from the EMP state rotates in the plane perpendicular to \vec{c} . For $\theta = 90^{\circ}$, that is, $\vec{k} \perp \vec{c}$, the far field thus appears partly linearly polarized. Therefore, eq 7 complements eqs 6a and 6b:

$$I^{\pi}(\theta) = I_{\uparrow\uparrow}^{\pi} + I_{\uparrow\downarrow}^{\pi} = 2A[K(B,\theta)\sin^2(\theta) + (1 - K(B,\theta))\sin^2(\theta)]$$
$$= 2A\sin^2(\theta) \tag{7}$$

This consideration results in a PL signal consisting of σ^+ , σ^- , and π components. Noticeably, because $I_{\uparrow\uparrow}^\pi=I_{\uparrow\downarrow}^\pi$ the overall component I^π is expected to be independent of magnetic field. We measure the π polarized PL emission by measuring $I(\alpha)$ with no quarter wave plate inserted into the optical beam. Without a quarter wave plate, circularly polarized components pass the analyzing linear polarizer by 50%, independent of the analyzer angular position α . Therefore any intensity change in the angular profile is due to a π polarized PL component. Figure 4b plots the angular dependence $I(\alpha)$ of the integrated PL intensity for cQD #1 in presence and absence of a magnetic field.

With no external magnetic field applied (black dots), $I(\alpha)$ exhibits an elongated shape with its maximum and minimum values at analyzer positions of $\alpha=25^\circ$ and 115° . The elongated shape is characteristic of the angular distribution of PL comprising a weak π polarized component superposed with a stronger circularly polarized component. The angular intensity dependence $I(\alpha)$ at B=5 T matches the intensity dependence at B=0 T very nicely in shape as well as in orientation, suggesting no change of the linear polarized PL component with magnetic field. This result shows that the π -

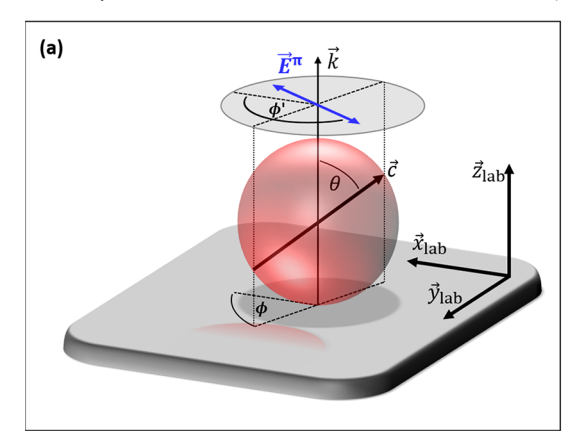
polarized component of the PL is independent of the distribution of EMPs formed along \vec{c} or $-\vec{c}$.

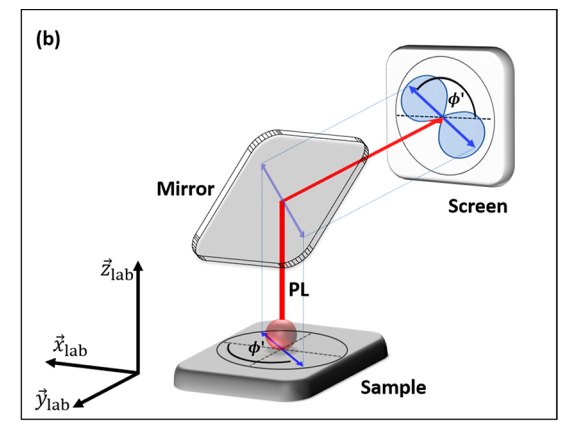
The degree of linear polarization is defined from the half axes a and b of the polarization ellipse as $\Delta I_{\rm lin}/I_{\rm lin}=(I_{\rm a}-I_{\rm b})/I_{\rm lin}$ $(I_a + I_b)$. From the minimal and maximal values of $I(\alpha)$, we estimate the degree of linear polarization as $\Delta I_{\rm lin}/I_{\rm lin}=15\%$, clearly proving the partly π polarized character of the PL from cQD #1. The orientation angle ϕ' of the polarization ellipse with respect to $\alpha = 0^{\circ}$ is given by an angle of maximum intensity, that is, $\phi'_{\#1} = 25^{\circ}$ in case of cQD #1. To test whether the angle of $\phi'_{\#1}$ is particular for cQD #1, Figure 4c compares $I(\alpha)$ for three single cQDs at B = 0 T. We find intensity profiles $I(\alpha)$ with individual strengths of the linear polarization contributions, $\Delta I_{\text{lin}}/I_{\text{lin}}$ = 15%, 29% and 42% for cQDs #1, #5, and #6, respectively. From eq 7, the strength of linearly polarized contributions is expected to depend on the polar angle θ between the crystal \vec{c} axis and the light propagation direction $k \| \vec{z}$. Therefore, the different strength of π -polarized PL components, that is, the different $\Delta I_{
m lin}/I_{
m lin}$, is a direct consequence of the individual polar angle θ between the crystal axis \vec{c} and the \vec{z} direction for each single cQD. The intensity profiles $I(\alpha)$ exhibit different linear polarization angles $\phi'_{\pm 1}$ = 25°, $\phi'_{#5} = 135$ °, and $\phi'_{#6} = 115$ ° for cQDs #1, #5, and #6. Thus, every cQD seems to exhibit a specific orientation of its linear polarized PL, which explains the characteristic deviation of $\Delta I/I$ from zero at B=0 (see Figure 4a and discussion of Figure S5 in the Supporting Information).

One elegant way to get the complete polarization state of the emission is to measure the full Stokes parameters (S_0, S_1, S_2, S_3) , defined by $S_0 = E_x E_x^* + E_y E_y^*$, $S_1 = E_x E_x^* - E_y E_y^*$, $S_2 = E_x E_y^* + E_y E_x^*$, and $S_3 = i(E_x E_y^* + E_y E_x^*)^{.70}$ Here $E_{x,y}^*$ are the complex conjugates of the complex electric field amplitudes $E_{x,y}$ in \vec{x} and \vec{y} directions. From the Stokes parameters, the exact degree of linear polarization (DLP), degree of circular polarization (DCP), and degree of total polarization (DOP) can be calculated by $DLP = \sqrt{S_1^2 + S_2^2}/S_0$, $DCP = S_3/S_0$, and $DOP = \sqrt{S_1^2 + S_2^2 + S_3^2}/S_0$. Additionally, the polarization angle ϕ' is given by $\phi' = 0.5$ atan (S_2/S_1) , offering very convenient access to ϕ' .

We therefore set up the appropriate Mueller matrices describing our experiment and measured the Stokes parameters as described in literature. ⁷⁰ Figure 4d plots the DLP, DCP, and DOP for single cQD #1. We first note that in case of cQD #1, the DCP trace is very similar to the trace of $\Delta I/I$. The DCP, however, starts exactly at zero for B = 0 T, while $\Delta I/I$ has a value of 2.5% at B=0 T. This finding demonstrates the advantage of using the DCP derived from the Stokes parameters as compared to simply using $\Delta I/I$. We additionally find that the DLP does not significantly change with B, in agreement with our conclusions earlier. The DOP on the other hand changes from being dominated by the DLP at zero field to being controlled by the DCP at high magnetic fields. Determining ϕ' from the Stokes parameters yields $\phi'_{\#1} = 30^{\circ}$, in close agreement with the value found from measuring the full angular intensity distribution $I(\alpha)$. Note that for the measurement of the Stokes parameters, merely four measurements are needed, significantly improving the efficiency of the experiment. These results represent the measurement of the complete polarization state for single cQD emission and showcase a robust method to characterize the polarization state for mixed polarization emission in (single) colloidal nanostructures.

Scheme 2. Illustration of (a) the cQD \vec{c} Axis Orientation, Described by the Polar Angle θ and Azimuthal Angle ϕ , and Its Impact on the Electric Field Orientation of Emitted Linearly Polarized Light^a and (B) the Correlation between the Sample Orientation in \vec{x} , \vec{y} and \vec{z} Lab Coordinates and the Intensity Pattern during the Measurement.





"Note that the polarization angle ϕ' of the electric field vector \vec{E} in the xy plane is perpendicular to the azimuthal angle ϕ , describing the direction of \vec{c} in the xy plane.

The full 3D orientation of the crystal \vec{c} axis is given by its polar angle θ with respect to the lab \vec{z} direction and by the azimuthal angle ϕ describing the angle between the projection of \vec{c} onto the xy plane and the \vec{x} direction of the substrate (see Scheme 2). The polar angle θ can be extracted from the measured DCP at high magnetic fields, while the azimuthal angle ϕ can be derived from the linear polarization angle ϕ' using $\phi = \phi' - 90^\circ$. Thus, the complete crystal 3D orientation of a single cQD in the lab coordinates can now be determined to a high degree of accuracy by accessing the full polarization state of QD emission and extracting θ and ϕ . Using the above given values of $\theta = 60^\circ$ from Figure 3f and $\phi' = 25^\circ$ from Figure 4b, we can calculate the normalized vector describing the \vec{c} axis of cQD #1 as

$$\vec{c}_{\text{QD}#1} = (\sin(\theta)\cos(\phi), \sin(\theta)\sin(\phi), \cos(\theta))^{\text{T}}$$

$$= (0.36, -0.78, 0.50)$$
(8)

Therefore, the measurement of the polarization angles ϕ and θ can directly be used to calculate cQD orientation on the substrate in the x, y, and z coordinates of the lab. This strategy can in principle be used to determine the crystal orientation in the lab reference frame for any anisotropic cQD, where one of the charge carriers' wave functions exhibits strong anisotropic character and the axis of anisotropy has sufficiently strong influence to constrain this charge carriers' wave function. The example of magnetically doped cQD provides a powerful illustration of this methodology due to the small magnetic fields needed to reach polarization saturation.

CONCLUSION

Single colloidal Mn²⁺-doped CdSe/CdS cQDs exhibiting EMP formation were investigated using polarization resolved magneto-PL spectroscopy. A magnetic field independent distinct linear polarization pattern is found for each cQD. While applying a magnetic field, the circular polarization degree of the PL is demonstrated to change characteristically for each single cQD, saturating at values <100%. A model based on the interplay between crystal anisotropy and magnetic exchange energy, including magnetic fluctuations, was developed to explain our findings. As a direct consequence

of a dominant anisotropy axis, we found a mixed polarization of the PL with significant linearly polarized contributions even at high magnetic fields. From a measurement of the magneticfield-dependent full Stokes parameters, the full polarization state of single cQD emission is extracted, and the degree of circular, linear, and total polarization is derived. Most important, we demonstrate that the full polarization state of single cQD emission can be used as a precise method to directly determine the crystal \vec{c} axis of the cQD in lab coordinates, a tool for extracting the exact 3D crystal orientation of a single anisotropic nanostructure by optical means. While cQDs with EMP formation are a nice material system to showcase this strategy, our approach is not exclusive to this material system, but is transferable to a variety of doped and undoped anisotropic colloidal semiconductor nanostructures.

METHODS

Sample Preparation. $\rm Mn^{2+}$:CdSe/CdS cQDs were synthesized as reported previously. 35,45,46,60 For single particle spectroscopy, the $\rm Mn^{2+}$:CdSe/CdS cQDs were dispersed in toluene, highly diluted, and spin-cast onto a $\rm SiO_2/Si$ substrate (oxide thickness: 270 nm), prepatterned with cross markers. Patterning of the substrate was done $\rm \it via$ electron beam lithography and thermal evapoaration of Ti/Au and served as a tool to reliable mark the position of single cQDs on the substrate, making it possible to find the same individual cQD several times. The dilution $(1:5 \times 10^5)$ was optimized to yield approximately one cQD per several $\rm \it \mu m^2$ to enable addressing single cQDs.

PL Spectroscopy. Micro-PL spectra were collected using a confocal microscope setup (Attocube atto CFM I) with a high numeric aperture objective (Attocube LT APO-Vis, NA: 0.82) inside a closed cycle cryostat ($T_{\rm sample}=4.0~{\rm K}$) with the option to apply magnetic fields up to 5 T in Faraday geometry. To ensure thermal contact to the reservoir, the samples were surrounded by helium exchange gas. For the PL experiments, a 532 nm solid-state laser (Laserglow LRS-0532 DPSS) was used as excitation source (power density <10 W/cm⁻², laser spot size on the sample: 700 nm) in combination with a laser clean up filter (Thorlabs FLH 532–10) and an ultrasteep long-pass edge filter (Razor Edge 532-RU). The spectra were recorded with a liquid nitrogen-cooled charge coupled device (CCD) camera (Horiba Symphony, back illuminated deep depletion 1-LS) in combination with a monochromator (Horiba Triax 550) equipped with a 150 mm⁻¹ grating.

Polarization Resolved PL Measurements. For polarization resolved PL experiments, a combination of a quarter wave plate (Thorlabs AQWP05M-580) and a rotatable linear polarizer (Thorlabs LPVISC050) were placed into the detection beam. The fast axis of the quarter wave plate was aligned horizontally (defined as $\alpha=0^{\circ}$) with respect to the optical table, and σ^+ and σ^- intensities were recorded with the linear polarizer at +45° and -45°, respectively. Gauging of the measurement setup was done by sending unpolarized light through the detection path (sample to detector).

For measurement of the Stokes parameters, the Mueller matrices of all optical components were determined by appropriate test measurements. 70 In addition to $I_{\rm wp}(45^\circ)$ (with quarter wave plate), three measurements $I(0^\circ)$, $I(45^\circ)$, and $I(90^\circ)$ were recorded without the quarter wave plate. According to the Mueller matrix describing our measurement setup, $S_0=1.18(I(0^\circ)+I(90^\circ))$, $S_1=1.18(I(0^\circ)-I(90^\circ))$, $S_2=2.35I(45^\circ)-S_0$, and $S_3=2.47I_{\rm wp}(45^\circ)-0.33I(45^\circ)-1.03(I(0^\circ)-I(90^\circ))$.

ASSOCIATED CONTENT

Supporting Information

The Supporting Information is available free of charge at https://pubs.acs.org/doi/10.1021/acsnano.1c04451.

QD analysis, PL spectra of the cQD ensemble, background discussion about isotropic and anisotropic EMP formation models, simulation parameters, discussion of finite $\Delta I/I$ at zero magnetic field (PDF)

AUTHOR INFORMATION

Corresponding Author

Gerd Bacher — Werkstoffe der Elektrotechnik and CENIDE, University of Duisburg-Essen, Duisburg 47057, Germany; orcid.org/0000-0001-8419-2158; Email: Gerd.Bacher@uni-due.de

Authors

Severin Lorenz – Werkstoffe der Elektrotechnik and CENIDE, University of Duisburg-Essen, Duisburg 47057, Germany

Jan Bieniek – Werkstoffe der Elektrotechnik and CENIDE, University of Duisburg-Essen, Duisburg 47057, Germany

Christian S. Erickson – Department of Chemistry, University of Washington, Seattle, Washington 98195-1700, United States; orcid.org/0000-0001-7888-0034

Daniel R. Gamelin — Department of Chemistry, University of Washington, Seattle, Washington 98195-1700, United States; © orcid.org/0000-0003-2888-9916

Rachel Fainblat – Werkstoffe der Elektrotechnik and CENIDE, University of Duisburg-Essen, Duisburg 47057, Germany; orcid.org/0000-0002-9488-2563

Complete contact information is available at: https://pubs.acs.org/10.1021/acsnano.1c04451

Notes

The authors declare no competing financial interest.

ACKNOWLEDGMENTS

S.L., R.F., and G.B. acknowledge the Deutsche Forschungsgemeinschaft (DFG) under contract BA 1422/22-1. We thank N. Stracke for the preparation of the patterned substrates by ebeam lithography, and we also thank J. Klein and H. Myja for their assistance with the illustration of the TOC graphic. This research was partially supported by the US National Science Foundation (NSF) through the UW Molecular Engineering Materials Center, a Materials Research Science and Engineer-

ing Center (DMR-1719797). Additional support from the US NSF (DMR-1807394) is gratefully acknowledged.

REFERENCES

- (1) Pirandola, S.; Eisert, J.; Weedbrook, C.; Furusawa, A.; Braunstein, S. L. Advances in Quantum Teleportation. *Nat. Photonics* **2015**, *9* (10), 641–652.
- (2) Sherson, J. F.; Krauter, H.; Olsson, R. K.; Julsgaard, B.; Hammerer, K.; Cirac, I.; Polzik, E. S. Quantum Teleportation between Light and Matter. *Nature* **2006**, *443* (7111), 557–560.
- (3) Togan, E.; Chu, Y.; Trifonov, A. S.; Jiang, L.; Maze, J.; Childress, L.; Dutt, M. V. G.; Sørensen, A. S.; Hemmer, P. R.; Zibrov, A. S.; Lukin, M. D. Quantum Entanglement between an Optical Photon and a Solid-State Spin Qubit. *Nature* **2010**, *466* (7307), 730–734.
- (4) Wagenknecht, C.; Li, C. M.; Reingruber, A.; Bao, X. H.; Goebel, A.; Chen, Y. A.; Zhang, Q.; Chen, K.; Pan, J. W. Experimental Demonstration of a Heralded Entanglement Source. *Nat. Photonics* **2010**, *4* (8), 549–552.
- (5) Degen, C. L.; Reinhard, F.; Cappellaro, P. Quantum Sensing. *Rev. Mod. Phys.* **2017**, 89 (3), 035002.
- (6) Gisin, N.; Ribordy, G.; Tittel, W.; Zbinden, H. Quantum Cryptography. *Rev. Mod. Phys.* **2002**, *74* (1), 145–195.
- (7) Zutic, I.; Fabian, J.; Das Sarma, S. Spintronics: Fundamentals and Applications. *Rev. Mod. Phys.* **2004**, *76* (2), 323–410.
- (8) Awschalom, D. D.; Flatté, M. E. Challenges for Semiconductor Spintronics. *Nat. Phys.* **2007**, *3* (3), 153–159.
- (9) Wolf, S. A; Awschalom, D. D.; Buhrman, R. A; Daughton, J. M.; von Molnár, S.; Roukes, M. L.; Chtchelkanova, A. Y.; Treger, D. M. Spintronics: A Spin-Based Electronics Vision for the Future. *Science* **2001**, 294 (5546), 1488–1495.
- (10) Ranjbar, B.; Gill, P. Circular Dichroism Techniques: Biomolecular and Nanostructural Analyses- A Review. *Chem. Biol. Drug Des.* **2009**, 74 (2), 101–120.
- (11) Longhi, G.; Castiglioni, E.; Koshoubu, J.; Mazzeo, G.; Abbate, S. Circularly Polarized Luminescence: A Review of Experimental and Theoretical Aspects. *Chirality* **2016**, 28 (10), 696–707.
- (12) Safronova, M. S.; Budker, D.; Demille, D.; Kimball, D. F. J.; Derevianko, A.; Clark, C. W. Search for New Physics with Atoms and Molecules. *Rev. Mod. Phys.* **2018**, *90* (2), 025008.
- (13) Tebyetekerwa, M.; Zhang, J.; Xu, Z.; Truong, T. N.; Yin, Z.; Lu, Y.; Ramakrishna, S.; Macdonald, D.; Nguyen, H. T. Mechanisms and Applications of Steady-State Photoluminescence Spectroscopy in Two-Dimensional Transition-Metal Dichalcogenides. *ACS Nano* **2020**, *14* (11), 14579–14604.
- (14) Chen, X.; Yan, T.; Zhu, B.; Yang, S.; Cui, X. Optical Control of Spin Polarization in Monolayer Transition Metal Dichalcogenides. ACS Nano 2017, 11 (2), 1581–1587.
- (15) Zhao, Y.; Zhang, S.; Shi, Y.; Zhang, Y.; Saito, R.; Zhang, J.; Tong, L. Characterization of Excitonic Nature in Raman Spectra Using Circularly Polarized Light. *ACS Nano* **2020**, *14* (8), 10527–10535.
- (16) De Luca, M.; Polimeni, A.; Capizzi, M.; Meaney, A. J.; Christianen, P. C. M.; Maan, J. K.; Mura, F.; Rubini, S.; Martelli, F. Determination of Exciton Reduced Mass and Gyromagnetic Factor of Wurtzite (InGa)as Nanowires by Photoluminescence Spectroscopy under High Magnetic Fields. ACS Nano 2013, 7 (12), 10717–10725.
- (17) Adhikari, S.; Spaeth, P.; Kar, A.; Baaske, M. D.; Khatua, S.; Orrit, M. Photothermal Microscopy: Imaging the Optical Absorption of Single Nanoparticles and Single Molecules. *ACS Nano* **2020**, *14* (12), 16414–16445.
- (18) Ghali, M.; Ohtani, K.; Ohno, Y.; Ohno, H. Generation and Control of Polarization-Entangled Photons from GaAs Island Quantum Dots by an Electric Field. *Nat. Commun.* **2012**, 3 (1), 661.
- (19) Fujita, T.; Morimoto, K.; Kiyama, H.; Allison, G.; Larsson, M.; Ludwig, A.; Valentin, S. R.; Wieck, A. D.; Oiwa, A.; Tarucha, S. Angular Momentum Transfer from Photon Polarization to an Electron Spin in a Gate-Defined Quantum Dot. *Nat. Commun.* **2019**, *10* (1), 2991.

- (20) Efros, A. L. Fine Structure and Polarization Properties of Band-Edge Excitons in Semiconductor Nanocrystals. In *Nanocrystal Quantum Dots*; Klimov, V. I., Ed.; CRC Press: Boca Raton, FL, 2010.
- (21) Htoon, H.; Furis, M.; Crooker, S. A.; Jeong, S.; Klimov, V. I. Linearly Polarized 'Fine Structure' of the Bright Exciton State in Individual CdSe Nanocrystal Quantum Dots. *Phys. Rev. B: Condens. Matter Mater. Phys.* **2008**, 77 (3), 035328.
- (22) Hu, J.; Li, Ls; Yang, W.; Manna, L.; Wang, Lw; Alivisatos, A. P. Linearly Polarized Emission from Colloidal Semiconductor Quantum Rods. *Science* **2001**, 292 (5524), 2060–2063.
- (23) Isarov, M.; Tan, L. Z.; Bodnarchuk, M. I.; Kovalenko, M. V.; Rappe, A. M.; Lifshitz, E. Rashba Effect in a Single Colloidal CsPbBr₃ Perovskite Nanocrystal Detected by Magneto-Optical Measurements. *Nano Lett.* **2017**, *17* (8), 5020–5026.
- (24) Becker, M. A.; Vaxenburg, R.; Nedelcu, G.; Sercel, P. C.; Shabaev, A.; Mehl, M. J.; Michopoulos, J. G.; Lambrakos, S. G.; Bernstein, N.; Lyons, J. L.; Stöferle, T.; Mahrt, R. F.; Kovalenko, M. V.; Norris, D. J.; Rainò, G.; Efros, A. L. Bright Triplet Excitons in Caesium Lead Halide Perovskites. *Nature* **2018**, 553 (7687), 189–193.
- (25) Efros, A.; Rosen, M.; Kuno, M.; Nirmal, M.; Norris, D.; Bawendi, M. Band-Edge Exciton in Quantum Dots of Semiconductors with a Degenerate Valence Band: Dark and Bright Exciton States. *Phys. Rev. B: Condens. Matter Mater. Phys.* **1996**, 54 (7), 4843–4856.
- (26) Furis, M.; Hollingsworth, J. A.; Klimov, V. I.; Crooker, S. A. Time- and Polarization-Resolved Optical Spectroscopy of Colloidal CdSe Nanocrystal Quantum Dots in High Magnetic Fields. *J. Phys. Chem. B* **2005**, *109* (32), 15332–15338.
- (27) Htoon, H.; Crooker, S. A.; Furis, M.; Jeong, S.; Efros, A. L.; Klimov, V. I. Anomalous Circular Polarization of Photoluminescence Spectra of Individual CdSe Nanocrystals in an Applied Magnetic Field. *Phys. Rev. Lett.* **2009**, *102* (1), 017402.
- (28) Rice, W. D.; McDaniel, H.; Klimov, V. I.; Crooker, S. A. Magneto-Optical Properties of CuInS₂ Nanocrystals. *J. Phys. Chem. Lett.* **2014**, 5 (23), 4105–4109.
- (29) Fu, M.; Tamarat, P.; Huang, H.; Even, J.; Rogach, A. L.; Lounis, B. Neutral and Charged Exciton Fine Structure in Single Lead Halide Perovskite Nanocrystals Revealed by Magneto-Optical Spectroscopy. *Nano Lett.* **2017**, *17* (5), 2895–2901.
- (30) Shornikova, E. V.; Biadala, L.; Yakovlev, D. R.; Feng, D.; Sapega, V. F.; Flipo, N.; Golovatenko, A. A.; Semina, M. A.; Rodina, A. V.; Mitioglu, A. A.; Ballottin, M. V.; Christianen, P. C. M.; Kusrayev, Y. G.; Nasilowski, M.; Dubertret, B.; Bayer, M. Electron and Hole g-Factors and Spin Dynamics of Negatively Charged Excitons in CdSe/CdS Colloidal Nanoplatelets with Thick Shells. *Nano Lett.* **2018**, *18* (1), 373–380.
- (31) Tamarat, P.; Bodnarchuk, M. I.; Trebbia, J. B.; Erni, R.; Kovalenko, M. V.; Even, J.; Lounis, B. The Ground Exciton State of Formamidinium Lead Bromide Perovskite Nanocrystals Is a Singlet Dark State. *Nat. Mater.* **2019**, *18* (7), 717–724.
- (32) Pandya, R.; Steinmetz, V.; Puttisong, Y.; Dufour, M.; Chen, W. M.; Chen, R. Y. S.; Barisien, T.; Sharma, A.; Lakhwani, G.; Mitioglu, A.; Christianen, P. C. M.; Legrand, L.; Bernardot, F.; Testelin, C.; Chin, A. W.; Ithurria, S.; Chamarro, M.; Rao, A. Fine Structure and Spin Dynamics of Linearly Polarized Indirect Excitons in Two-Dimensional CdSe/CdTe Colloidal Heterostructures. *ACS Nano* **2019**, *13* (9), 10140–10153.
- (33) Furdyna, J. K.; Kossut, K. Dilute Magnetic Semiconductors. In *Semiconductors and Semimetals*; Furdyna, J. K., Kossut, J., Ed.; Academic Press, Inc.: New York, 1988; Vol. 25, pp R29–R64.
- (34) Knowles, K. E.; Nelson, H. D.; Kilburn, T. B.; Gamelin, D. R. Singlet—Triplet Splittings in the Luminescent Excited States of Colloidal Cu⁺:CdSe, Cu⁺:InP, and CuInS₂ Nanocrystals: Charge-Transfer Configurations and Self-Trapped Excitons. *J. Am. Chem. Soc.* **2015**, *137* (40), 13138–13147.
- (35) Nelson, H. D.; Bradshaw, L. R.; Barrows, C. J.; Vlaskin, V. A.; Gamelin, D. R. Picosecond Dynamics of Excitonic Magnetic Polarons in Colloidal Diffusion-Doped Cd_{1-x}Mn_xSe Quantum Dots. *ACS Nano* **2015**, *9* (11), 11177–11191.

- (36) Delikanli, S.; Akgul, M. Z.; Murphy, J. R.; Barman, B.; Tsai, Y.; Scrace, T.; Zhang, P.; Bozok, B.; Hernández-Martínez, P. L.; Christodoulides, J.; Cartwright, A. N.; Petrou, A.; Demir, H. V. Mn²⁺ -Doped CdSe/CdS Core/Multishell Colloidal Quantum Wells Enabling Tunable Carrier—Dopant Exchange Interactions. *ACS Nano* **2015**, 9 (12), 12473—12479.
- (37) Nelson, H. D.; Hinterding, S. O. M.; Fainblat, R.; Creutz, S. E.; Li, X.; Gamelin, D. R. Mid-Gap States and Normal vs Inverted Bonding in Luminescent Cu⁺- and Ag⁺-Doped CdSe Nanocrystals. J. Am. Chem. Soc. **2017**, 139 (18), 6411–6421.
- (38) Najafi, A.; Tarasek, S.; Delikanli, S.; Zhang, P.; Norden, T.; Shendre, S.; Sharma, M.; Bhattacharya, A.; Taghipour, N.; Pientka, J.; Demir, H. V.; Petrou, A.; Thomay, T. CdSe/CdMnS Nanoplatelets with Bilayer Core and Magnetically Doped Shell Exhibit Switchable Excitonic Circular Polarization: Implications for Lasers and Light-Emitting Diodes. ACS Appl. Nano Mater. 2020, 3 (4), 3151–3156.
- (39) Barman, B.; Pientka, J. M.; Murphy, J. R.; Cartwright, A. N.; Chou, W. C.; Fan, W. C.; Oszwałdowski, R.; Petrou, A. Circular Polarization Dynamics during Magnetic Polaron Formation in Type-II Magnetic Quantum Dots. *J. Phys. Chem. C* **2020**, *124* (23), 12766–12773
- (40) Shornikova, E. V.; Yakovlev, D. R.; Tolmachev, D. O.; Ivanov, V. Y.; Kalitukha, I. V.; Sapega, V. F.; Kudlacik, D.; Kusrayev, Y. G.; Golovatenko, A. A.; Shendre, S.; Delikanli, S.; Demir, H. V.; Bayer, M. Magneto-Optics of Excitons Interacting with Magnetic Ions in CdSe/CdMnS Colloidal Nanoplatelets. *ACS Nano* **2020**, *14* (7), 9032–9041.
- (41) Klopotowski; Mikulski, J.; Szymura, M.; Minikayev, R.; Parlińska-Wojtan, M.; Kazimierczuk, T.; Kossut, J. Ultraslow Spin Relaxation Dynamics in Colloidal Copper-Doped CdSe Quantum Dots. J. Phys. Chem. C 2020, 124, 1042–1052.
- (42) Najafi, A.; Sharma, M.; Delikanli, S.; Bhattacharya, A.; Murphy, J. R.; Pientka, J.; Sharma, A.; Quinn, A. P.; Erdem, O.; Kattel, S.; Kelestemur, Y.; Kovalenko, M. V.; Rice, W. D.; Demir, H. V.; Petrou, A. Light-Induced Paramagnetism in Colloidal Ag⁺-Doped CdSe Nanoplatelets. *J. Phys. Chem. Lett.* **2021**, *12*, 2892–2899.
- (43) Henneberger, F.; Puls, J. Diluted Magnetic Quantum Dots. In Introduction to the Physics of Diluted Magnetic Semiconductors; Kossut, K., Gaj, J. A., Eds.; Springer: Heidelberg, 2010.
- (44) Furdyna, J. K. Diluted Magnetic Semiconductors. J. Appl. Phys. 1988, 64 (4), R29.
- (45) Vlaskin, V. A.; Barrows, C. J.; Erickson, C. S.; Gamelin, D. R. Nanocrystal Diffusion Doping. J. Am. Chem. Soc. 2013, 135 (38), 14380–14389.
- (46) Barrows, C. J.; Vlaskin, V. A.; Gamelin, D. R. Absorption and Magnetic Circular Dichroism Analyses of Giant Zeeman Splittings in Diffusion-Doped Colloidal Cd_{1-x}Mn_xSe Quantum Dots. *J. Phys. Chem. Lett.* **2015**, *6* (15), 3076–3081.
- (47) Gaj, J. A. Semiconductors and Semimetals; Furdyna, J. K., Kossut, J., Ed.; Academic Press: San Diego, CA, 1988; Vol. 25.
- (48) Hundt, A.; Puls, J.; Henneberger, F. Spin Properties of Self-Organized Diluted Magnetic Cd_{1-x}Mn_x Quantum Dots. *Phys. Rev. B: Condens. Matter Mater. Phys.* **2004**, *69* (12), 121309.
- (49) Fainblat, R.; Frohleiks, J.; Muckel, F.; Yu, J. H.; Yang, J.; Hyeon, T.; Bacher, G. Quantum Confinement-Controlled Exchange Coupling in Manganese(II)-Doped CdSe Two-Dimensional Quantum Well Nanoribbons. *Nano Lett.* **2012**, *12* (10), 5311–5317.
- (50) Muckel, F.; Yang, J.; Lorenz, S.; Baek, W.; Chang, H.; Hyeon, T.; Bacher, G.; Fainblat, R. Digital Doping in Magic-Sized CdSe Clusters. ACS Nano 2016, 10 (7), 7135–7141.
- (51) Beaulac, R.; Ochsenbein, S. T.; Gamelin, D. R. Colloidal Transition-Metal-Doped Quantum Dots. In *Nanocrystal Quantum Dots*; Klimov, V. I., Ed.; CRC Press: Boca Raton, FL, 2010; pp 397–453
- (52) Merkulov, I. A.; Kavokin, K. V.; Mackh, G.; Kuhn-Heinrich, B.; Ossau, W.; Waag, A.; Landwehr, G.; Yakovlev, D. R. Luminescence Polarization and Spontaneous Lowering of Symmetry Caused by Magnetic-Polaron Formation in Semimagnetic-Semiconductor Quantum Wells. *Phys. Solid State* **1997**, *39* (11), 1859–1863.

- (53) Keller, D.; Yakovlev, D. R.; König, B.; Ossau, W.; Gruber, T.; Waag, A.; Molenkamp, L. W.; Scherbakov, A. V. Heating of the Magnetic Ion System in (Zn, Mn)Se/(Zn, Be)Se Semimagnetic Quantum Wells by Means of Photoexcitation. *Phys. Rev. B: Condens. Matter Mater. Phys.* **2001**, 65 (3), 035313.
- (54) Reshina, I. I.; Ivanov, S. V. Magnetooptical Properties of a Single CdMnSe/CdMgSe Quantum Well. *Semiconductors* **2008**, 42 (11), 1318–1322.
- (55) Akimov, I. A.; Godde, T.; Kavokin, K. V.; Yakovlev, D. R.; Reshina, I. I.; Sedova, I. V.; Sorokin, S. V.; Ivanov, S. V.; Kusrayev, Y. G.; Bayer, M. Dynamics of Exciton Magnetic Polarons in CdMnSe/CdMgSe Quantum Wells: Effect of Self-Localization. *Phys. Rev. B: Condens. Matter Mater. Phys.* **2017**, *95* (15), 155303.
- (56) Merkulov, I. A.; Yakovlev, D. R.; Kavokin, K. V.; Mackh, G.; Ossau, W.; Waag, A.; Landwehr, G. Hierarchy of Relaxation Times in the Formation of an Excitonic Magnetic Polaron in (CdMn)Te. *JETP Letters.* 1995, 62 (4), 335.
- (57) Merkulov, I. A.; Pozina, G. R.; Coquillat, D.; Paganotto, N.; Siviniant, J.; Lascaray, J. P.; Cibert, J. Parameters of the Magnetic Polaron State in Diluted Magnetic Semiconductors Cd-Mn-Te with Low Manganese Concentration. *Phys. Rev. B: Condens. Matter Mater. Phys.* 1996, 54 (8), 5727–5731.
- (58) Beaulac, R.; Schneider, L.; Archer, P. I.; Bacher, G.; Gamelin, D. R. Light-Induced Spontaneous Magnetization in Doped Colloidal Quantum Dots. *Science* **2009**, 325 (5943), 973–976.
- (59) Rice, W. D.; Liu, W.; Pinchetti, V.; Yakovlev, D. R.; Klimov, V. I.; Crooker, S. A. Direct Measurements of Magnetic Polarons in Cd_{1-x}Mn_xSe Nanocrystals from Resonant Photoluminescence. *Nano Lett.* **2017**, *17* (5), 3068–3075.
- (60) Lorenz, S.; Erickson, C. S.; Riesner, M.; Gamelin, D. R.; Fainblat, R.; Bacher, G. Directed Exciton Magnetic Polaron Formation in a Single Colloidal Mn²⁺:CdSe/CdS Quantum Dot. *Nano Lett.* **2020**, 20 (3), 1896–1906.
- (61) Johnston-Halperin, E.; Awschalom, D. D.; Crooker, S. A.; Efros, A. L.; Rosen, M.; Peng, X.; Alivisatos, A. P. Spin Spectroscopy of Dark Excitons in CdSe Quantum Dots to 60 T. *Phys. Rev. B: Condens. Matter Mater. Phys.* **2001**, 63 (20), 205309.
- (62) Granados Del Águila, A.; Pettinari, G.; Groeneveld, E.; De Mello Donegá, C.; Vanmaekelbergh, D.; Maan, J. C.; Christianen, P. C. M. Optical Spectroscopy of Dark and Bright Excitons in CdSe Nanocrystals in High Magnetic Fields. *J. Phys. Chem. C* **2017**, *121* (42), 23693–23704.
- (63) Yakovlev, D. R.; Ossau, W.; Landwehr, G.; Bicknell-Tassius, R. N.; Waag, A.; Uraltsev, I. N. First Observation and Experimental Proof of Free Magnetic Polaron Formation in CdTe/(Cd, Mn)Te Quantum Wells. *Solid State Commun.* 1990, 76 (3), 325–329.
- (64) Yakovlev, D. R. Exciton Magnetic Polarons in Semimagnetic Quantum Wells and Superlattices. *J. Phys. IV* **1993**, 3 (5), 67–74.
- (65) Maksimov, A. A.; Bacher, G.; McDonald, A.; Kulakovskii, V. D.; Forchel, A.; Becker, C. R.; Landwehr, G.; Molenkamp, L. W. Magnetic Polarons in a Single Diluted Magnetic Semiconductor Quantum Dot. *Phys. Rev. B: Condens. Matter Mater. Phys.* **2000**, 62 (12), R7767–R7770.
- (66) Empedocles, S. A.; Norris, D. J.; Bawendi, M. G. Photoluminescence Spectroscopy of Single CdSe Nanocrystallite Quantum Dots. *Phys. Rev. Lett.* **1996**, *77* (18), 3873–3876.
- (67) Fernée, M. J.; Littleton, B. N.; Cooper, S.; Rubinsztein-Dunlop, H.; Gómez, D. E.; Mulvaney, P. Acoustic Phonon Contributions to the Emission Spectrum of Single CdSe Nanocrystals. *J. Phys. Chem. C* **2008**, *112*, 1878–1884.
- (68) Dorozhkin, P. S.; Chernenko, A. V.; Kulakovskii, V. D.; Brichkin, A. S.; Maksimov, A. A.; Schoemig, H.; Bacher, G.; Forchel, A.; Lee, S.; Dobrowolska, M.; Furdyna, J. K. Longitudinal and Transverse Fluctuations of Magnetization of the Excitonic Magnetic Polaron in a Semimagnetic Single Quantum Dot. *Phys. Rev. B: Condens. Matter Mater. Phys.* 2003, 68 (19), 195313.
- (69) Archer, P. I.; Santangelo, S. A.; Gamelin, D. R. Direct Observation of sp-d Exchange Interactions in Colloidal Mn²⁺- and

- Co²⁺-Doped CdSe Quantum Dots. *Nano Lett.* **2007**, 7 (4), 1037–1043.
- (70) Goldstein, D. H. Polarized Light, 3rd ed.; CRC Press: Boca Raton, FL, 2011.